Hydrogen−Deuterium Exchange in Free and Prodomain-Complexed Subtilisin[†]

Nese Sari, Biao Ruan, Kathryn E. Fisher, Patrick A. Alexander, John Orban, and Philip N. Bryan*

Center for Advanced Research in Biotechnology, University of Maryland Biotechnology Institute, 9600 Gudelsky Drive, Rockville, Maryland 20850

Received August 7, 2006; Revised Manuscript Received November 13, 2006

ABSTRACT: Residue-specific exchange rates of 223 amide protons in free and prodomain-complexed subtilisin were determined in order to understand how the prodomain binding affects the energetics of subtilisin folding. In free subtilisin, amide protons can be categorized according to exchange rate: 74 fast exchangers (rates ≥ 1 h^{-1}); 52 medium exchangers (rates between 1 h^{-1} and 1 day^{-1}); 31 slow exchangers (rates between 1 day^{-1} and 0.001 day^{-1}). The remaining 66 amide proteins did not exchange detectibly over 9 months (k_{obs} < year^{-1}) and were denoted as core protons. Core residues occur throughout the main structural elements of subtilisin. Prodomain binding results in high protection factors (100−1000) in the central β-sheet, particularly in the vicinity of β-strands S5, S6, and S7 and the connecting loops between them. These connecting loops provide the ligands to the cation at metal site B. Overall, prodomain binding seems to facilitate the organization of the entire central β-sheet and α-helix C in the left-handed crossover connection between β-strands two and three. It also appears to facilitate the isomerization of multiple prolines late in folding, allowing the formation of metal site B. The gain of stability region around site B comes at the cost of stability in regions more distal to prodomain binding: the *C*-terminal α-helix H and the *N*-terminal α-helices A and B. The acceleration of exchange in these regions by prodomain binding reveals an antagonism between the folding intermediate and the full native structure. This antagonism helps to explain why the prodomain is needed to stabilize the folding intermediate as well as why the unfolding of free subtilisin seldom occurs via this intermediate.

In order to better understand the role of the prodomain in subtilisin folding, we have determined hydrogen−deuterium exchange rates for free subtilisin and subtilisin in complex with its prodomain. The exchange rates of 223 amide protons were determined. The basic principle is that main chain amide protons that are hydrogen bonded in a stable secondary or tertiary structure will exchange with deuterons in the solvent slower than the protons in dynamic regions (*1*−*4*). In general, the slowest exchanging amide protons have energies of opening consistent with the free energy of global unfolding and are referred to as the slow-exchanging core of the protein (*5*). The opening rates of faster-exchanging amides can be used to determine ΔG values for partial unfolding events and have been used to understand folding mechanisms for many facile-folding proteins (*6*−*14*). Our goal is to define the equilibrium between folded, partially folded, and unfolded states in subtilisin. The advantages in characterizing the stability of a slow-folding protein such as subtilisin in this manner are that the system remains at equilibrium (with rare unfolding events detected by the exchange of protons with deuterons) and measurements are made under native conditions (so that no extrapolations from denaturing conditions are required). NMR analysis also allows residue-specific unfolding rates to be determined, providing structural information about the intermediate states. Such native state H−D exchange studies have previously been carried out on the uncomplexed form of α-lytic protease in order to understand the origins of its kinetic barrier to folding and unfolding (*15*).

Previous X-ray-crystallographic studies on the subtilisin−prodomain complex have revealed that the bound prodomain is a single compact domain with an antiparallel four-stranded β-sheet and two three-turn α-helices (Figure 1) (*16*, *17*). The β-sheet of the prodomain packs tightly against the two parallel surface α-helices of subtilisin (helix D, 104−116 and helix E, 133−144). Prodomain residues E69 and D71 form helix caps for the *N*-termini of subtilisin helices D and E. In another charge dipole interaction, the carboxylate of E112 of subtilisin accepts H bonds from the peptide nitrogens of prodomain residues 42−44. The *C*-terminal residues 72−77 extend out from the central part of the prodomain and bind in a substrate-like manner along subtilisin's active site cleft. Residues Y77, A76, H75, and A74 of the prodomain occupy subsites S1, S2, S3, and S4 of subtilisin, respectively. Almost all of the prodomain's contacts are made with subtilisin residues 100−144. The subtilisin structure in complex with proR9[1] is very similar to its uncomplexed

[†] This work was supported by NIH Grant GM42560 and the W. M. Keck Foundation.

* Corresponding author. Tel: 240-314-6220. Fax: 240-314-6255. E-mail: bryan@umbi.umd.edu.

[1] Abbreviations: A shorthand for denoting mutation is used. For example, S221A is serine at position 221 substituted with alanine; proR9, subtilisin BPN′ prodomain with the following mutations: the substitution of amino acids 17−21 (TMSTM) with SGIK and the subtitutions A23C, K27E, V37L, Q40C, H72K, and H75K; Sbt70, subtilisin BPN′ with the following mutations: K43N, M50F, A73L, Δ75-83, Q206V, Y217K, N218S, and S221A; Tris, Tris(hydroxymethyl)amino-methane.

10.1021/bi061601r CCC: $37.00
Published on Web 12/21/2006

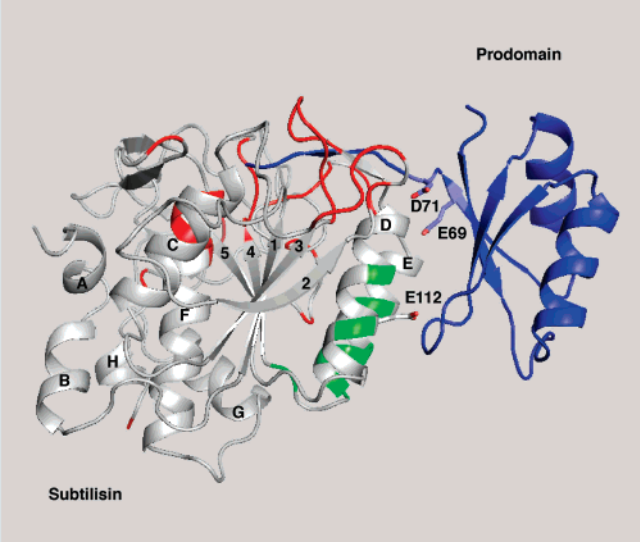

FIGURE 1: Ribbon drawing of the Sbt70−proR9 complex (1spb). ProR9 is in blue. Amide protons in Sbt70, which were missing in the free protein but visible in the complex, are shown in red. Amide protons, which were visible in the free Sbt70 but missing in the complex, are shown in green. The α-helix capping amino acids of the prodomain (E69 and D71) and the *β*-bend capping amino acid of subtilisin (E112) are also shown with labels. Helices A−H are denoted with capital letters, and *β*-strands 1−5 are numbered.

structure but exhibits minor movements in the substrate binding region. In particular, the distance between residues 101−102 and 127−128 in the substrate-binding region decreases by almost 1 Å compared to that in uncomplexed subtilisin.

We have shown previously that the prodomain accelerates subtilisin folding by stabilizing an intermediate on the folding pathway. Once the intermediate forms, it acts as a folding nucleus with subsequent folding propagating into other regions. Using transient state kinetic experiments, it has been possible to determine microscopic rate constants for the binding of the prodomain to unfolded subtilisin and also the isomerization rate of the bimolecular intermediate into the native complex ((*18*) and preceding article). Because of the stability of the native complex, however, it has not been possible to measure its stability relative to the intermediate complex and the unfolded state in the kinetic experiments. Because transiently populated species can be observed in H−D exchange studies, they allow us to probe the structure of the intermediate state stabilized by prodomain binding and measure its stability relative to the native state.

MATERIALS AND METHODS

Subtilisin Sbt70. The basic engineered version of subtilisin that we used is denoted Sbt70 (K43N, M50F, Δ75-83, A73L, Q206V, Y217K, N218S, and S221A). Sbt70 is a variant subtilisin engineered for facile folding (*19*). It was uniformly labeled with ^{15}N and ^{13}C (≥95%) by growing *E. coli* containing the expression plasmid in M9 minimal media with $^{15}NH_4Cl$ as the sole nitrogen source and ^{13}C-glucose as the sole carbon source. Purification was as described (*18*).

Prodomain Pro9. The basic engineered version of the subtilisin prodomain that we used is denoted proR9 (A23C, K27E, V37L, Q40C, H72K, and H75K and T17, M18, S19, T20, and M21 replaced with SGIK). ProR9 was engineered to be independently stable ($\Delta G_{folding} = -4$ kcal/mol in 0.1 M KPi at pH 7.0 and 25 °C) and monomeric to high concentrations ($K_d = 0.5$ mM in 0.1 M KPi at pH 7.0 and 25 °C) (*18*, *20*). ProR9 is unlabeled in these experiments and was purified as described (*18*).

Resonance Assignments. NMR spectra were acquired at 318 K in States-TPPI mode on Bruker DMX-600 spectrometers equipped with either a *z*-gradient triple resonance (^{1}H, ^{13}C, and ^{15}N) cryoprobe or a conventional 3-axis triple resonance probe. Pulsed field gradients were used for coherence selection and solvent suppression. Data were processed using nmrPipe and analyzed with Sparky (Goddard, T. D., and Kneller, D. G., UCSF). Backbone assignments were made in both Sbt70 and the Sbt70−proR9 complex using a ^{13}C/^{15}N-labeled Sbt70 sample and standard HNCO, HNCACB, CBCA(CO)NH, and HBHA(CO)NH triple resonance experiments. The assignments will be described elsewhere.

Hydrogen Exchange: The rate of hydrogen−deuterium (H−D) exchange of 0.7 mM Sbt70 in stoichiometric complex with proR9 was monitored in 0.2 M KPO_4 at pH 7.2. Samples were maintained at 37 °C throughout the time course, except for data collection, which was performed at 45 °C. The higher temperature was used for data collection to narrow line widths and improve the signal-to-noise ratio. The first ^{1}H-^{15}N HSQC spectra were collected immediately after rehydration of the samples with D_2O. Spectra were collected every 10 days for the first 2 months and then every month thereafter for 9 months.

RESULTS

The NMR experiments described here were performed on a mutant subtilisin (Sbt70), which was previously engineered for facile folding. Studies of the complex were carried out with Sbt70 complexed to a stabilized version of the prodomain denoted proR9. Sbt70 contains the mutation S221A, which decreases peptidase activity by ∼10^6-fold, and six stabilizing substitutions (K43N, M50F, A73L, Δ75-83, Q206V, Y217K, and N218S) (*19*). None of the mutant amino acids except residue 221 contact the prodomain in the bimolecular complex (*16*). These variants were used in our analysis because we were able to measure uncatalyzed folding rates for Sbt70 alone and the microscopic rate constants for all steps in its bimolecular folding reaction with proR9 (*18*).

Assignment of Amide Protons. Of the 266 main chain amide protons in Sbt70, 29 were missing from the ^{1}H-^{15}N HSQC spectra of both free Sbt70 and the complex. ProR9 is unlabeled and spectrally invisible in these experiments. The missing Sbt70 peaks correspond to the amides primarily in loop regions. This observation indicates that these loops undergo conformational exchange on an intermediate time scale, resulting in the loss of signal due to exchange broadening. Certain main chain amides visible in the complex were not observed in the free enzyme. These were primarily in the vicinity of the substrate-binding pocket (Figure 1). These positions acquire a well-defined chemical environment upon binding the *C*-terminal tail of proR9 but are exchange-broadened in the absence of substrate interactions. Amino acids 109, 112, 113, 138, 141, 142, 144, and 147 were seen in free Sbt70 but not observed in the complex. These occur at the interface between proR9 and Sbt70 helices D and E.

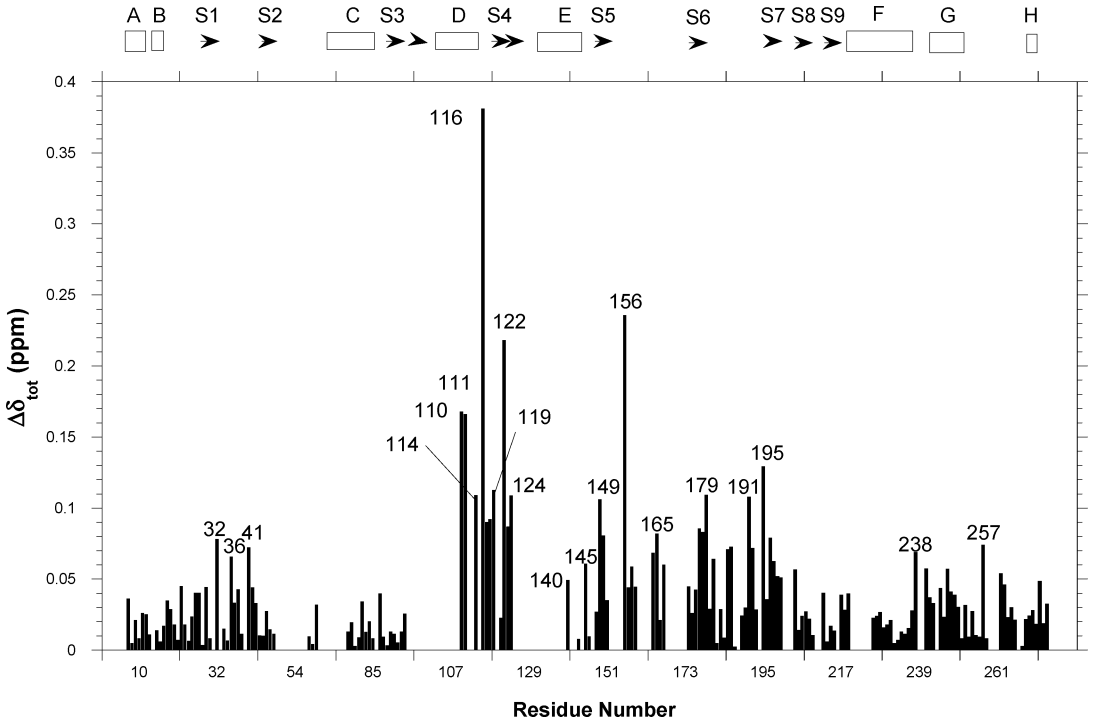

FIGURE 2: Weighted sum of ^{15}N and ^{1}H chemical shift differences between Sbt70 and the Sbt70−proR9 complex vs residue number. The secondary structure (top) was based on the X-ray structure of the complex (1spb) (*16*).

It was assumed that the position of proR9 is somewhat mobile in this region and results in exchange-broadened peaks. The chemical shift differences between Sbt70 and the complex are shown in Figure 2. The pattern suggests that the transmission of conformational effects extends well beyond the contact surface.

H−D Exchange. We have collected the ^{1}H-^{15}N HSQC spectra of both free Sbt70 and the complex as a function of time in D_2O and determined opening rates for 223 individual hydrogen bonds (Figure 3A−D). According to the structural unfolding model, the rate of exchange of a core proton is determined by the relative rate of folding and unfolding (k_f and k_u) and the intrinsic proton exchange rate in the unfolded protein (k_{int}) as follows (*21*), where $S_{(H)}$ is native subtilisin with main chain amides bonded to protons, $U_{(H)}$ is unfolded subtilisin with main chain amides bonded to protons, $U_{(D)}$ is unfolded subtilisin with main chain amides exchanged for deuterons, and $S_{(D)}$ is native subtilisin with main chain amides exchanged for deuterons.

$$\mathbf{S_{(H)} \overset{k_u}{\underset{k_f}{\Leftrightarrow}} U_{(H)} \overset{k_{int}\ (D_2O)}{\Leftrightarrow} U_{(D)} \overset{k_f}{\underset{k_u}{\Leftrightarrow}} S_{(D)}}$$

The observed rate of exchange (k_{obs}) depends upon the intrinsic exchange rate in the unfolded state (k_{int}), the folding rate (k_f), and unfolding rate (k_u) for an individual amide proton, according to the following equation.

$$k_{obs} = k_u k_{int}/(k_f + k_{int})$$

If k_f is much faster than k_{int}, then the observed rate of exchange will approximately equal k_{int} divided by the equilibrium constant for folding (k_f/k_u). If k_f is slow compared to k_{int}, then the overall rate of exchange for this class of protons should equal k_u.

Amide protons are grouped according to exchange rate: 74 fast exchangers (rates ≥ 1 h^{-1}); 52 medium exchangers (rates between 1 h^{-1} and 1 day^{-1}); 31 slow exchangers (rates between 1 day^{-1} and 0.001 day^{-1}). The remaining 66 amide protons did not exchange detectibly over 9 months (k_{obs} > year^{-1}) and were denoted as core protons. These core residues occur throughout the main structural elements of subtilisin, except for the short *N*-terminal α-helices (A and B) and *β*-strands 8 and 9 (Figure 4).

H−D Exchange in the Sbt70 Complex. To find out how the prodomain changes the energetics of subtilisin folding, exchange rates in free and complexed Sbt70 were compared. If the prodomain binds to native Sbt70 more tightly than it binds to any intermediate, then the rate of exchange of all core amide protons in subtilisin should be slowed in the bound state relative to the free state. The magnitude of the highest protection factors obtained can be related to the binding affinity from the following relationship (*22*):

$$1/\text{protection factor} = k_{free}/k_{complex} = ([\text{complex}]/K_d)^{1/2}$$

where K_d is the dissociation constant for prodomain binding. As described in the following section, the highest protection factors occur at the interface and exceed 10^5. If the exchange rate of some amide protons in Sbt70 increases in the complex, however, this would indicate that partial unfolding events are catalyzed by proR9 binding and that proR9 binds more tightly to an intermediately folded state of Sbt70 than it does to the native state.

Protons Whose Exchange Is Slowed in the Complex. Protection through Direct Contact with proR9. The amide proton of A134 at the *N*-terminal end of helix E has a protection factor of $>10^5$ in the complex. In free Sbt70, this

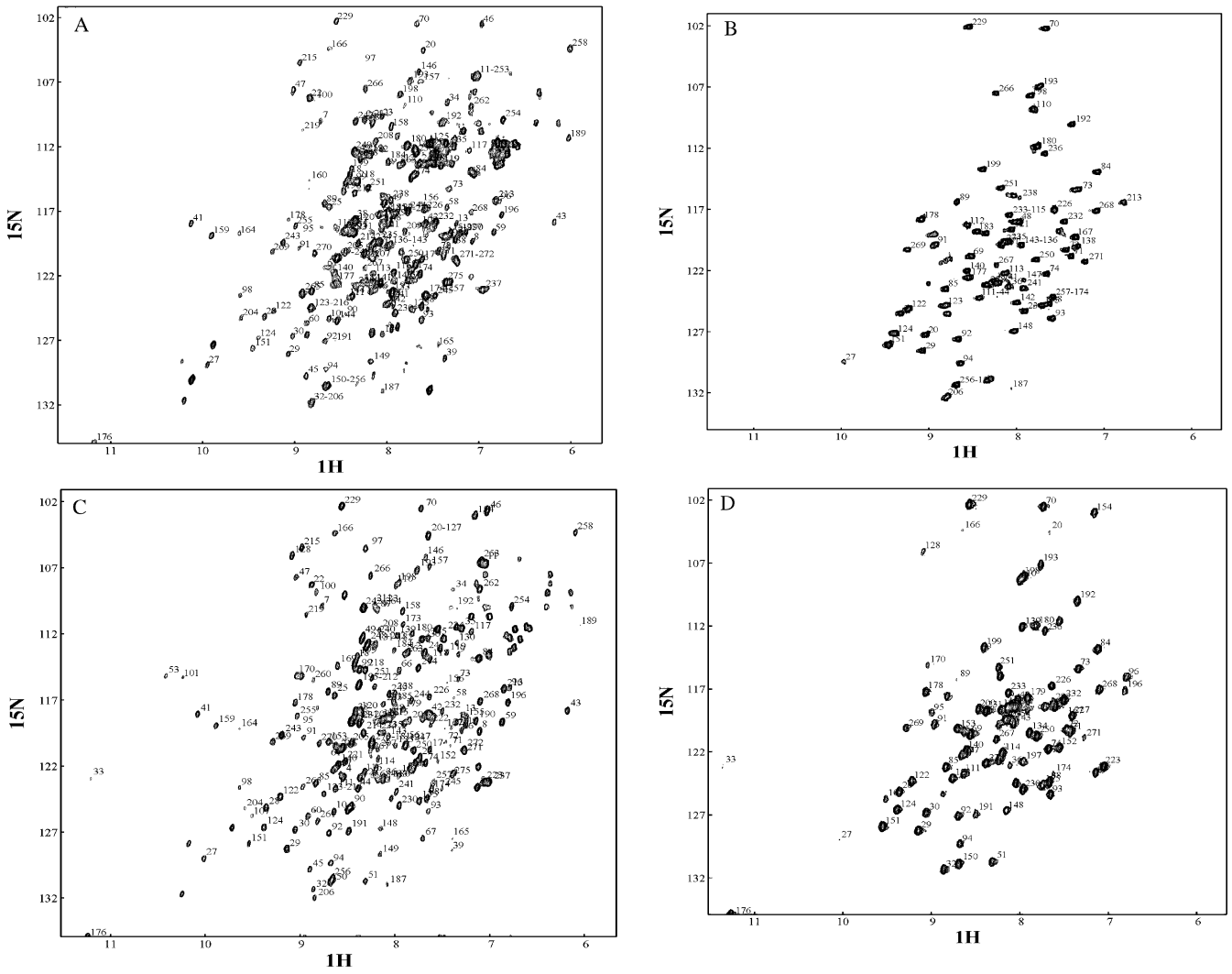

FIGURE 3: (A) ^{15}N-HSQC spectra of Sbt70 in H_2O. (B) ^{15}N-HSQC spectra of Sbt70 after 20 days in D_2O. (C) ^{1}H-^{15}N HSQC spectrum of the Sbt70−proR9 complex in H_2O. (D) ^{1}H-^{15}N HSQC spectrum of the Sbt70−proR9 complex after 20 days in D_2O.

amide is H-bonded to Oγ of S132 in a helix-capping interaction. In the complex, the Oϵ of the proR9 residue E69 replaces the helix-capping H bond of S132 (Figure 5). A second helix-capping interaction of the Sbt70 residue S105 in helix D is formed by Oδ of proR9 residue D71. No capping H bond is observed in the crystal structure of free Sbt70. Amide protons for residues 102−106 are not seen in either the free or the proR9 complex, however, indicating conformational heterogeneity in this region. Thus, proR9 appears to make a very strong H bond with the end of helix E and a weaker H bond with the end of helix D. We also note that another charge−dipole interaction between E112 of Sbt70 and the NH's of proR9 residues 42, 43, and 44 also results in exchange broadening of subtilisin amides in the vicinity of E112.

Residues 72−77 of proR9 bind in the substrate-binding cleft and become the central strand in an antiparallel β-sheet with Sbt70 strands 100−103 and 125−128. Amide protons of Sbt70 amino acids G102, Y104, and G127 are H bonded to proR9 in the complex. The exchange rate of G127 is >1 h^{-1}, whereas the peaks for G102 and Y104 are exchange broadened, indicating that the proR9 tail undergoes breathing motions in the complex at 45 °C.

The exchange of some H-bonds in Sbt70 helices D and E at the hydrophobic interface with proR9 are slowed significantly (5−50 fold). Even higher protection factors (100−1000) are seen in the central β-sheet, particularly in the vicinity of β-strands S5, S6, and S7 and the two connecting loops between them, (153−174) and (181−197) (Figure 5). These connecting loops provide all the ligands to the metal at site B: carbonyl oxygen atoms of G169, Y171, V174, and E195 and the side chain carboxylate oxygen of D197. Protection factors of 100−1000 for these residues correspond to a $\Delta\Delta G_{opening}$ of 3−4 kcal/mol in the complex relative to that of free Sbt70. Many core protons are also likely to undergo slowed exchange, but the changes are not manifest because no exchange is observed in either the free or the complexed state over the nine-month time course.

Protons Whose Exchange Is Accelerated in the Complex. The gain of stability in this S5−S7 region of the structure comes at the cost of stability in regions more distal to proR9 binding: the *C*-terminal helix H and the *N*-terminal helices A and B. We note also that the amide of V270, which forms an interdomain H bond with the carbonyl oxygen of I11, is destabilized. This is a rare instance in which a main chain H bond spans two distant elements of secondary structure. Other destabilized areas included fraying of the end of the S1 and S5 β-strands (K27 NH to D120 Oδ1) and fraying of the end of helix F (I234 NH to H238 CO). The magnitude

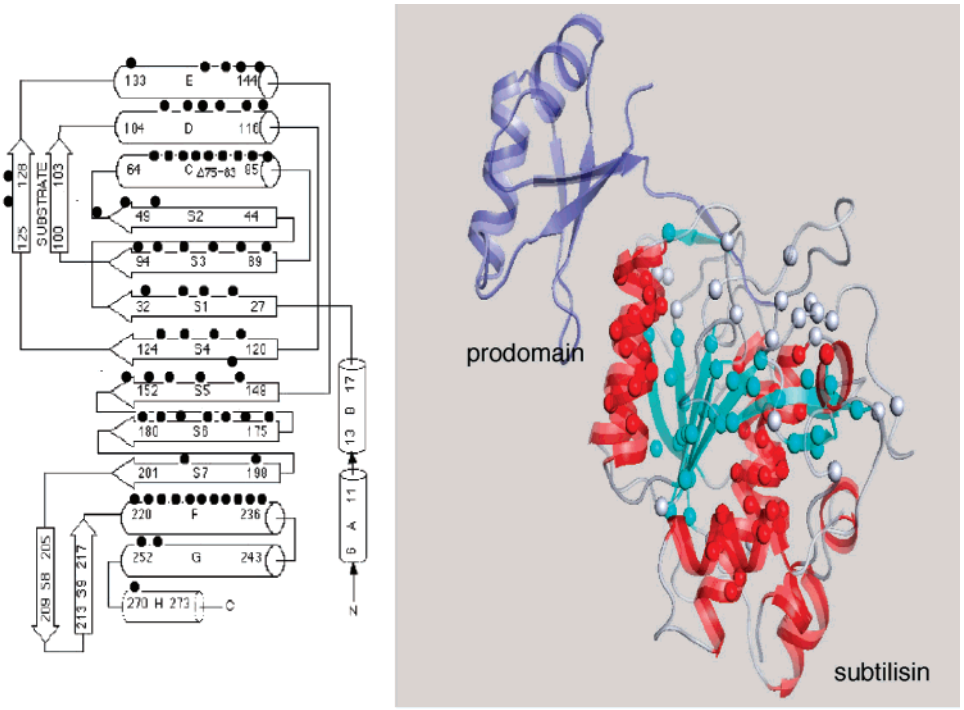

FIGURE 4: Schematic representation of Sbt70 topology. (A) The positions of the 66 slowest-exchanging (core) amide protons in Sbt70 are shown as black dots. This Figure was adapted from ref 32 (*32*). The slowest-exchanging protons reside throughout the central seven-stranded parallel β-sheet and in all of the five major α-helical segments (C−G). (B) The core amides are shown as spheres in the subtilisin structure in α-helices, red; in the β-sheet, cyan; and in the loops, gray.

of the accelerated exchange is between 5- and 50-fold (Figure 6).

DISCUSSION

Estimation of ΔG *for Global Unfolding.* The 66 slowest-exchanging amide protons exchange at a rate of $<\text{year}^{-1}$. The folding of Sbt70 occurs at a rate of 0.0033 s^{-1} in Sbt70 (0.2 M KPi at pH 7.2) (*23*). Assuming that the exchange of core protons reflects the global unfolding rate, the ratio of folding to unfolding rates of core amides yields a $\Delta G_{\text{unfolding}} > 7$ kcal/mol (0.2 M KPi at pH 7.2). The concentration of potassium ions in this buffer is 0.34 M. The binding constant of site B for potassium is 1×10^4 M^{-1}. The contribution of potassium binding to $\Delta G_{\text{unfolding}}$ can be calculated to be ~5 kcal/mol using the equation $\Delta G_{\text{binding}} = RT \ln(1+ K_A[\text{potassium}])$ (*24*). Thus, a significant portion of the energy barrier to Sbt70 unfolding is contributed by cation binding. In subtilisin with an intact calcium site A (e.g., S221A subtilisin), cation binding contributes significantly more of the energy barrier to unfolding. The binding energy contributed to the free energy of unfolding at [calcium] = 100 mM is 13.5 kcal/mol. At low ionic strength (30 mM Tris-HCl at pH 7.2), S221A subtilisin unfolds spontaneously ($k_{\text{unfolding}} = 0.6$ h^{-1}). Calcium binding creates such a large effect on the unfolding energy because neither of the two cation sites is formed until late in the folding process (preceding article).

Stabilization of the Folding Intermediate by proR9. Almost all of the proR9's contacts with Sbt70 are made with residues 100−144, which includes helices D and E and the substrate binding strands 100−103 and 125−128 (*16*). The exchange rates of numerous amide protons in the contact area are slowed. The region of high protection factors extends beyond the direct contact area into the metal site B region: β-strands S5, S6, and S7 and the two connecting loops. It is known that proR9 accelerates folding by binding to and stabilizing the folding intermediate as well as by accelerating the conversion of the intermediate to the native state (*18*). Several previous experimental observations help explain and place the H−D exchange results in context: (1) proR9 binding to the intermediate is independent of the isomeric forms of the 14 prolines in subtilisin ((*18*) and the preceding article); (2) proR9 binding to the intermediate is independent of cation concentration (*19*, *25*, *26*); (3) the kinetics of folding of the bimolecular intermediate into the native complex is determined by the rate of proline isomerization (preceding article). Because proR9 accelerates the conversion of the bimolecular intermediate into the native intermediate, it follows that proR9 accelerates proline isomerization. The cation independence of the formation of the bimolecular intermediate indicates that metal site B is formed during the isomerization step. We would suggest, therefore, that the barrier between the intermediate complex and the native complex is created by the need for proline isomerization of several prolines to create site B. The formation of site B would appear to require prolines 168, 172, and 194 to be in their native isomeric form (cis, trans, and trans, respectively), with little stabilization from cation binding achieved until this occurs. ProR9 binding may, therefore, stabilize the loops and increase the probability of the simultaneous occurrence of all three native proline isomers. This stabilization is reflected in the slowed exchange of amide protons in the S5−S7 region of the protein.

ProR9 binding has little effect on protection factors in the long central helix F and the adjacent helix G and actually destabilizes the *C*-terminal helix H and the *N*-terminal helices A and B. Destabilization can be discerned from the patterns of H−D exchange in free and complexed subtilisin. Although amide exchange in the S5−S7 strands and the intervening

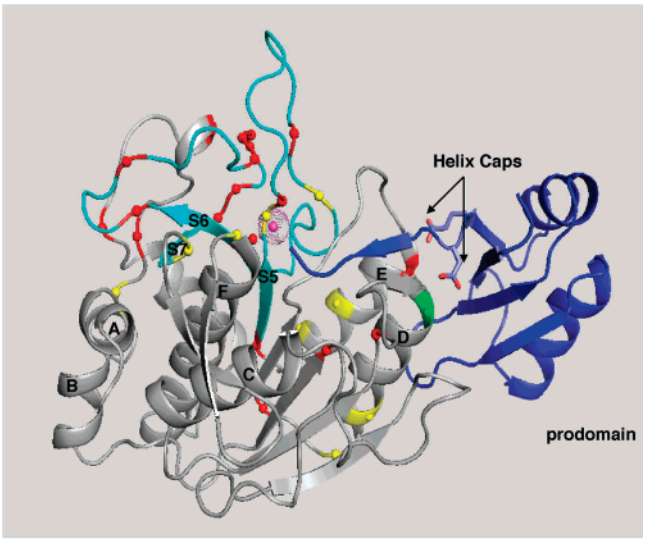

FIGURE 5: Protection pattern in the Sbt70−proR9 complex. ProR9 is in blue. The β-strands S5−S7 and the intervening loops are shown in turquoise. Amide protons that are strongly protected (100−1000×) by proR9 binding are shown in red. More weakly protected amides (5−20×) are shown in yellow. The potassium bound at site B is shown in magenta. α-helices are denoted by capital letters, according to the order in which they appear in the linear sequence (Figure 4). The helix-capping residues of the prodomain (E69 and D71) are indicated with arrows. Amides of subtilisin residues at the end at helix D (105 shown in green) and helix E (134 is shown in red) are hydrogen bonded to the capping residues.

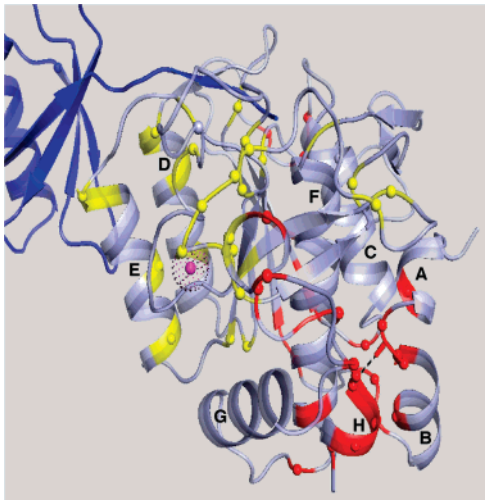

FIGURE 6: Ribbon diagram of the Sbt70−proR9 complex. ProR9 is in blue. Amino acids whose exchange is slowed by proR9 binding are shown in yellow. Amino acids whose exchange is accelerated by proR9 binding are shown in red. The potassium bound at site B is shown in magenta. α-helices are denoted by capital letters, according to the order in which they appear in the linear sequence (Figure 4). The hydrogen bond between the amide of V270 at the end of helix H and the CO of I11 at the end of helix B is indicated by a dashed line.

connections are slowed by proR9 binding, amides in the *N*- and *C*-terminal portions of the molecule exchange faster in the complex than in the free enzyme, indicating that proR9 stabilizes an intermediate structure that is antagonistic to the fully native structure. Mutagenesis data also strongly implicate helix C as part of the intermediate structure ((*18*, *19*, *27*, *28*) and the preceding article). Helix C is part of the left-handed crossover connection between β-strands S2 and S3. Overall, proR9 binding seems to facilitate the organization of the entire seven-stranded central β-sheet. ProR9 binds very tightly to the native state (K_d ~0.1 nM), and the PN complex is more stable than the PI complex. Nevertheless, the pattern of exchange rate shows that the stability of N relative to I is less in the complex than in free Sbt70.

Antagonism between the Intermediate and the Native State. The antagonism between the folding intermediate (I) and the native state (N) and the resultant effects on folding rate can be understood by considering a simple equilibrium.

$$U \underset{\leftarrow}{\overset{K_{U\ to\ I}}{\rightarrow}} I \underset{\leftarrow}{\overset{K_{I\ to\ N}}{\rightarrow}} N + metal \underset{\leftarrow}{\overset{K_{metal}}{\rightarrow}} N(metal)$$

Subtilisin folds with the intermediate forming first in a conformation whose structured regions are slightly nonnative. The native state is stabilized by metal binding, but the stability of I is independent of metal concentration. The position of the I to N equilibrium determines the folding rate, with higher stability of I leading to faster folding. The stability of the native state is also influenced by the position of the I to N equilibrium, but higher stability of I leads to a less stable native state because I has a suboptimal interface with the rest of the molecule in the native state.

We suggest that the intermediate state is preferentially stabilized by proR9 binding and leads to the protection pattern in the complex in which some amide protons are protected while others exchange faster. The fact that the equilibrium from I to N is altered by proR9 binding suggests that it might also be altered by mutation. Furthermore, the mechanism predicts that the effects of mutations that favor one state relative to the other will be dependent on metal concentration. We have previously analyzed a number of stabilizing mutations in subtilisin that support this model (*29*). Stabilizing mutations fall into one of three classes. The largest class of mutations stabilize subtilisin only in the presence of excess metal. A smaller number of mutations stabilize independently of metal concentration, and a few mutations stabilize only in low concentrations of metal (*29*). According to the model, mutations that stabilize only in the presence of excess metal concentration stabilize the N state relative to I because the metal sites form only in the last stages of folding. Some mutations stabilize independently of metal concentration because the I and N states share structural features, and some mutations increase their stabilities to the same extent. The mutations that stabilize only when metal concentration is low appear to stabilize the I state relative to N and also would be predicted to increase the folding rate because they would favor the formation of the intermediate. Examples of mutations in this class are F50M, T22C-S87C, and Δ75-83. The mutation M50F results in a small increase in folding rate (~3-fold). The mutations 22-87C and Δ75-83 result in very large increases in folding rate (*30*, *31*). Note that the positions of mutations accelerating folding is consistent with the idea that the intermediate includes the central β-sheet and helix C.

The antagonism between a folding intermediate and the native state observed in subtilisin raises the question, Does high kinetic stability to unfolding necessarily lead to slow folding rates? Theoretically, the answer would be no. If the complementarity between I and N were perfect such that interactions in I were completely accommodated in N, then

the energetic barrier between the native state and the intermediate could be maintained without destabilizing the intermediate. If, however, the folding of I into N requires some relaxation of interactions within I, then the high independent stability of I would compromise the stability of the whole. This phenomenon may be more likely to occur in a large, cooperative protein structure such as subtilisin in which achieving perfect shape complementarity between all structural elements may be difficult. Lower stability of individual portions would distribute stresses throughout the molecule and result in a highly cooperative folding reaction. The antagonism also helps to explain why the prodomain is needed to stabilize the folding intermediate as well as why the unfolding of free subtilisin seldom occurs via this intermediate.

It is possible, however, that the evolution of subtilisin in the presence of the prodomain may have allowed the antagonistic situation to arise out of opportunity rather than necessity because subtilisin, unlike most proteins, had no selective pressure to fold independently.

ACKNOWLEDGMENT

We thank Edward Eisenstein, John Moult, and Bradley Anderson for helpful discussions.

REFERENCES

1. Englander, S. W. (2000) Protein folding intermediates and pathways studied by hydrogen exchange. *Annu. Rev. Biophys. Biomol. Struct. 29*, 213−238.
2. Englander, S. W., et al. (1997) Hydrogen exchange: the modern legacy of Linderstrom-Lang, *Protein Sci. 6*, 1101−1109.
3. Englander, S. W., et al. (1996) Mechanisms and uses of hydrogen exchange, *Curr. Opin. Struct. Biol. 6*, 18−23.
4. Englander, S. W., Downer, N. W., and Teitelbaum, H. (1972) Hydrogen exchange, *Annu. Rev. Biochem. 41*, 903−924.
5. Woodward, C. K. (1994) Hydrogen exchange rates and protein folding. *Curr. Opin. Struct. Biol. 4*, 112−116.
6. Xu, Y., Mayne, L., and Englander, S. W. (1998) Evidence for an unfolding and refolding pathway in cytochrome *c*. *Nat. Struct. Biol. 5*, 774−778.
7. Kragelund, B. B., et al. (1998) Mapping the lifetimes of local opening events in a native state protein. *Protein Sci. 7*, 2237−2248.
8. Raschke, T. M., and Marqusee, S. (1997) The kinetic folding intermediate of ribonuclease H resembles the acid molten globule and partially unfolded molecules detected under native conditions (published erratum appears in *Nat. Struct. Biol. 4*, 505), *Nat. Struct. Biol. 4*, 298−304.
9. Chung, E. W., et al. (1997) Hydrogen exchange properties of proteins in native and denatured states monitored by mass spectrometry and NM. *Protein Sci. 6*, 1316−1324.
10. Arrington, C. B., and Robertson, A. D. (1997) Microsecond protein folding kinetics from native-state hydrogen exchange, *Biochemistry 36*, 8686−8691.
11. Miranker, A., et al. (1996) Investigation of protein folding by mass spectrometry, *FASEB J. 10*, 93−101.
12. Chamberlain, A. K., Handel, T. M., and Marqusee, S. (1996) Detection of rare partially folded molecules in equilibrium with the native conformation of RNaseH, *Nat. Struct. Biol. 3*, 782−787.
13. Jones, B. E., and Matthews, C. R. (1995) Early intermediates in the folding of dihydrofolate reductase from *Escherichia coli* detected by hydrogen exchange and NMR. *Protein Sci. 4*, 167−177.
14. Bai, Y., et al. (1995) Protein folding intermediates: native-state hydrogen exchange, *Science 269*, 192−197.
15. Jaswal, S. S., et al. (2002) Energetic landscape of alpha-lytic protease optimizes longevity through kinetic stability, *Nature 415*, 343−346.
16. Gallagher, T. D., et al. (1995) The prosegment-subtilisin BPN′ complex: crystal structure of a specific foldase, *Structure 3*, 907−914.
17. Jain, S. C., et al. (1998) The crystal structure of an autoprocessed Ser221Cys-subtilisin E-propeptide complex at 2.0 Å resolution, *J. Mol. Biol. 284*, 137−144.
18. Ruan, B., Hoskins, J., and Bryan, P. (1999) Rapid folding of calcium-free subtilisin by a stabilized pro-domain mutant, *Biochemistry 38*, 8562−8571.
19. Bryan, P., et al. (1995) Catalysis of a protein folding reaction: Mechanistic implications of the 2.0 Å structure of the subtilisin-prodomain complex, *Biochemistry 34*, 10310−10318.
20. Ruan, B., et al. (1998) Stabilizing the subtilisin BPN′ pro-domain by phage display selection: how restrictive is the amino acid code for maximum protein stability? *Protein Sci. 7*, 2345−2353.
21. Roder, H. (1989) Structural characterization of protein folding intermediates by proton magnetic resonance and hydrogen exchange, *Methods Enzymol. 176*, 446−489.
22. Paterson, Y., Englander, S. W., and Roder, H. (1990) An antibody binding site on cytochrome *c* defined by hydrogen exchange and two-dimensional NMR, *Science 249*, 755−759.
23. Bryan, P. N. (1995) Subtilisin Engineered for Facile Folding: Analysis of Uncatalyzed and Prodomain-Catalyzed Folding, in *Intramolecular Chaperones and Protein Folding* (Shinde, U., and Inouye, M., Eds.) pp 85−112, R. G. Landes, Austin, TX.
24. Alexander, P. A., Ruan, B., and Bryan, P. N. (2001) Cation-dependent stability of subtilisin, *Biochemistry 40*, 10634−10639.
25. Ruvinov, S., et al. (1997) Engineering the independent folding of the subtilisin BPN′ prodomain: Analysis of two-state folding vs. protein stability, *Biochemistry 36*, 10414−10421.
26. Wang, L., et al. (1995) Prodomain mutations at the subtilisin interface: correlation of binding energy and the rate of catalyzed folding, *Biochemistry 34*, 15415−15420.
27. Strausberg, S., et al. (1993) Catalysis of a protein folding reaction: thermodynamic and kinetic analysis of subtilisin BPN′ interactions with its propeptide fragment, *Biochemistry 32*, 8112−8119.
28. Bryan, P., et al. (1992) Energetics of folding subtilisin BPN′, *Biochemistry 31*, 4937−4945.
29. Alexander, P. A., et al. (2001) Stabilizing mutations and calcium-dependent stability of subtilisin, *Biochemistry 40*, 10640−10644.
30. Strausberg, S., et al. (1993) An engineered disulfide crosslink accelerates the refolding rate of calcium-free subtilisin by 850-fold, *Biochemistry 32*, 10371−10377.
31. Bryan, P. N. (1992) Engineering Dramatic Increases in the Stability of Subtilisin, in *Pharmaceutical Biotechnology* (Ahern, T. J., and Manning, M. C., Eds.) pp 147−181, Plenum Press, New York.
32. Siezen, R. J., et al. (1991) Homology modelling and protein engineering strategy of subtilases, the family of subtilisin-like serine proteinases, *Protein Eng. 4*, 719−737.

BI061601R